Structural Monitoring and Maintenance, *Vol. 8, No. 2 (2021) 167-186*
DOI: https://doi.org/10.12989/smm.2021.8.2.167

Unscented Kalman filter approach for tracking physical and dynamic properties of structures: Validation for multi-story buildings under seismic excitation

Carlos A. Gaviria*[1] and Luis A. Montejo [2]

[1] *Civil Engineering Program, Facultad de Estudios a Distancia, Universidad Militar Nueva Granada, Colombia*
[2] *Department of Engineering Sciences and Materials, University of Puerto Rico at Mayaguez, Puerto Rico*

(*Received October 16, 2020, Revised January 13, 2020, Accepted May 21, 2021*)

Abstract. An improved unscented Kalman filter approach is implemented to estimate induced displacements and changes in structural properties (stiffness, frequencies and damping) during the forced dynamic response of multistory buildings to seismic excitations. The methodology is validated using a fiber-based nonlinear model of a 4-story 4-bays reinforced concrete (RC) frame building subjected to a set of earthquakes causing different levels of inelastic demand on the structure. The variation of the dynamic properties is successfully estimated by iterative updating the filter parameters. The estimated peak values of stiffness and damping reached during the seismic excitation agree with peak inelastic demand values and seem appropriate for detection and damage diagnosis of RC structures.

Keywords: health monitoring; kalman filter; reinforced concrete; earthquake; multiple degree of freedom; openSees

1. Introduction

Identification of sudden damage episodes during strong motion excitations has been a first feature of vibration-based structural health monitoring (SHM) schemes (Murillo *et al*. 2019, Yazdanpanah *et al*. 2020). Nevertheless, identification of the location and level of damage on multiple degree of freedom systems exhibiting nonlinear hysteretic behavior has been a more evasive target. Methodologies based on the identification and comparison of the dynamic properties before and after the strong motion excitation are limited in application as the observed changes saturate at large levels of inelastic demand (Consuegra and Irfanoglu 2008, Montejo *et al*. 2008, 2015). By contrast, instantaneous identification (i.e., at each instant of the seismic event) of displacements, stiffness and damping provide robust indicators of the level of damage induced in the structure (Gaviria and Montejo 2019).

There are several Kalman filter (KF) algorithms that has been studied over the last years within SHM approaches to identify real time variations of the structural parameters. This Bayesian identification approach can deal with the uncertainties in modeling and measuring (De Roeck 2019,

*Corresponding author, Associate Professor, E-mail: carlos.gaviria@unimilitar.edu.co

http://www.techno-press.org/?journal=smm&subpage=7 ISSN: 2288-6605 (Print), 2288-6613 (Online)

Astroza *et al*. 2020). Wu and Wang (2014) found that unscented Kalman filter (UKF) method generate the best estimation stiffness and damping coefficient per floor compare with extended Kalman filter (EKF) approach for identification of parameters of a Bouc–Wen hysteretic model using only simulated accelerations responses at each degree of freedom (DOF). Kuleli and Nagayama (2020) implement a stochastic approximation scheme along with the unscented Kalman filter (UKF-RM) for rubber bearing stiffness on different sides of the girder considering multi-support excitation. Results show that by automatically updating the filter statistics, system states are successfully estimated with a fast convergence rate. Qiu and Lau (2021) investigated the effect of vehicle noise on acoustic-laser technique on detection of delamination or debonding in Fiber-reinforced polymer (FRP) concrete panels. The proposed de-noising scheme applied shows that detection of large defect is more exposed to vehicle noise. The UKF has been used to determine the model parameters of an experimental nonlinear energy sink (a passive control device) by Lund *et al*. (2020). They demonstrated that geometric non-linearity in its stiffness and a friction-based nonlinearity in its damping on control device are well identified in a Latin hypercube sampling process with Bayesian inference techniques. However, consideration must also be given on global sensitivity analysis to establishing the identifiability of the model with respect to a particular excitation signal (Lund *et al*. 2019). Bocciarelli and Ranzi (2020) limited the possible influence of a weak a priori knowledge of the model parameters and error in the previous instant estimation of the system response of an implemented extended Kalman filter (EKF). They found that the influence of exposure conditions and thickness on temperature, relative humidity and shrinkage induced deformations of concrete elements are well estimated. The performance of an EKF is compared with a particular filter algorithm within an unknown inputs' perspective by Wan *et al*. (2018). The results from numerical simulations of a 3DOF nonlinear elastic structure and a 4DOF hysteretic structure illustrate that both approaches are capable of identifying the states and parameters. Similarly, Sen *et al*. (2018) tested an interacting Particle-Kalman filter with a second filter that fed the estimated seismic force back to the KF and a new gain matrix for correlated process and measurement noises. Numerical simulations demonstrated successful identification of damage and stability at any point in time. Alternatively, an iterative least-square and UKF is combined to identify the stiffness of elements and damage features using only limited measured response time histories by Katkhuda *et al*. (2017). They were able to identify damaged and undamaged states on steel framed structures instrumented with a minimum number of sensors. In addition, to deal with the relatively large number of degrees of freedom, Azam and Mariani (2018) and Azam *et al*. (2017) proposed extended Kalman filter and hybrid extended Kalman particle filter as framework. Satisfactory performance was observed in terms of tracked variation of the stiffness, stability of the estimates, and robustness against inaccuracies. However, the location and quantification of damage was spatially smeared or averaged by the reduced-order model scheme.

Damage diagnosis based on calibration of nonlinear Finite element (FE) models has ascended as an attractive approach intended to localize and to qualify the damage (De Roeck 2019). Roohi *et al*. (2021) proposed a framework that combines a FE model of a structure and acceleration measurements. The dissipated energy is used as a feature for damage detection and localization. The framework identified the location of main damage in severe damage columns (beam/column joints) located at the fourth floor on a seven-story reinforced concrete building. He *et al*. (2019) selected the maximum and minimum strains of section fibers as target parameters in a RC pier model constructed in OpenSees. The numerical results depicted that the updated model is able to predict future performance of the structure after an earthquake. Alternatively, Astroza *et al*. (2017) uses the EKF and UKF as recursive Bayesian estimation methods to update the estimation of the

FE model. Results on data numerically simulated of a RC frame building (Astroza *et al*. 2017), steel frame building and isolated bridge (Li *et al*. 2017, Astroza *et al*. 2019, 2020) show close agreement with the target nonlinear material constitutive parameters. However, important misfits appear in no instrumented responses estimated at global and local levels (Astroza and Alessandri 2019).

Despite the many advances made in the field, highly nonlinear systems like RC structures subject to severe earthquake excitation are still challenging to identify (Lund *et al*. 2019). The UKF seems to be a prevailing tool for system identification but, slight variations on the parameters distribution may produce significant fluctuation in the estimated model properties (Lund *et al*. 2020). The identifiability of the model is conditioned by the capacity of the input signal to fully excite the structure (Lund *et al*. 2019) and its uses may be prohibitive for updating FE models of real-world structures due to its computational demand (Astroza *et al*. 2019). Current trend in KF approaches is to set the process and measurement noise covariance matrices constant over the assessment period within a manual tuning scheme. However, if the initial matrices are not well approximated, KF performances resulted in a suboptimal or even divergence way (Kuleli and Nagayama 2020).

The aim of this study is to extend the application of a UKF scheme that engages a simple nonparametric model proposed by Gaviria and Montejo (2019) for single-degree-of-freedom (SDOF) systems to multiple-degree-of-freedom (MDOF) systems. The extension of the UKF approach is validated using numerical responses of state of the art finite element fiber-based nonlinear RC frame model induced to different levels of inelastic demand by a group of scaled earthquakes. The estimated properties (physical/dynamic) are compared with the ductility demand of the whole system and each floor to evaluate the ability for damage assessment.

2. The unscented Kalman filter and the condensed system

The UKF is a method that has been used to produce the best estimation (statistically) of data that is not directly measured in the structure (i.e., stiffness, damping, displacements and others parameters) using noise contaminated raw-data (e.g., acceleration at each floor of a building (Gaviria and Montejo 2019, Song and Dyke 2014)). In this way, physical and dynamic properties within a UKF scheme can be estimated in an online mode as one of its major advantage over others techniques (e.g., Output-Only identification (Gaviria and Montejo 2016) or Wavelet-based damage detection approaches (Aguirre *et al*. 2013, Quiñones *et al*. 2015, Gaviria and Montejo 2018) without an additional de-noising scheme (e.g., Montejo and Vidot-Vega 2012, Qiu and Lau 2021). The UKF scheme proposed by Gaviria and Montejo (2019) was used to investigate the properties of a RC column modeled as a single degree of freedom SDOF system. In this situation, the result is one value of displacement, stiffness and damping at each discrete time instant. For the application to MDOF systems, the stiffness matrix should be estimated and a condensed stiffness matrix is engaged on the premise that only lateral acceleration is recorded. This reduced stiffness matrix takes into account the complete stiffness matrix as a result of a static condensation. Accordingly, the equilibrium equation of the MDOF system (Eq. (1) in Gaviria and Montejo (2019)) is write as Gaviria (2015)

$$[M_c]\{\ddot{u}\} + [C_c]\{\dot{u}\} + [K_c]\{u\} = -[M_c]\{r_c\}\{\ddot{u_g}\} \tag{1}$$

where $[M_c]$, $[C_c]$ and $[K_c]$ are matrices that represent the mass, damping and stiffness of system,

respectively; $\{r_c\}$, $\{u\}$, $\{\dot{u}\}$ and $\{\ddot{u}\}$ are vectors of influence coefficient (linked to each lateral instrumented floor), displacement, velocity and acceleration correspondingly; and, $\ddot{u}_g$ is the seismic acceleration at the soil level. Eq. (1) is a nonparametric representation of the nonlinear behavior of the structure that bypasses assumptions about its hysteretic behavior and covers a lot of possible behaviors (Masri *et al*. 2004, Ghanem and Ferro 2006). Also, it is reducing the computing time needed for an optimal real-time implementation due to the fact that parameters needed to estimate as less in contrast to complex nonlinear solutions (Gaviria and Montejo 2019). The static condensation procedure can be found elsewhere (Cheng 2001, He *et al*. 2014).

A reduced masses matrix $[M_c]$ with diagonal terms equal to the lumped mass by story is used since masses associated to rotational DOFs are negligible in dynamic analysis of frame-type structures. The Caughey damping matrix is introduced to avoid ill-conditioning on computing damping ratios and gives a separate damping ratio for each mode (Humar 2012). The time-variant model parameters and instantaneous model responses are well-arranged in a joint state vector xi, in order to implement the nonparametric model in a UKF approach

$$x_i = \left\{ {u_i}^T \quad {\dot{u}_i}^T \quad {\ddot{u}_i}^T \quad {ke_i}^T \quad {\xi e_i}^T \right\}^T \tag{2}$$

Where ke_i and ξe_i are respectively, vectors with the scaled exponent parameters of the stiffness and damping ratios (i.e., lateral stiffness $k_i = kc * exp(ke_i)$ and modal damping ratios $\xi_i = \xi c * exp(\xi e_i)$) at time t_i. T symbolizes the transpose. kc and ξc are the constant parameters vectors fixed to the initial values of the lateral stiffness and modal damping ratios on elastic range (i.e. $kc = k_0$, $\xi c = \xi_0$) thus, the scaled exponent parameters are zero on the linear range (i.e., $ke_0 = 0$, $\xi e_0 = 0$). The scaled exponential substitution on UKF procedure allows to estimate only positive values of parameters that ensure the consistency of the algorithm (Julier and Uhlmann 1997). In this study, the horizontal acceleration at each floor is assumed to be recorded and its UKF estimates are stored in the measurement vector y_i

$$y_\mathrm{i} = \ddot{u}_\mathrm{i} \tag{3}$$

The experimental recorded accelerations are collected in a vector called z. Thus, the estimated values of measured data (y_i) by the UKF are aims to meet the current values (z) by tuning parameters values in the state vector (x_i). The implementation of this nonparametric model in the UKF scheme follows the rules proposed by Gaviria and Montejo (2019) with the improvements for the MDOF system described in section 4.

2.1 The initial matrices to MDOF system

As was aforementioned, the implemented stiffness matrix in the Kalman filter is calculated by the static condensation of the initial linear-static assembly of the frame model by OpenSees software (i.e., before any lateral load is applied). The initial damping matrix is generated with damping ratios of 2 percent for all modes, which corresponds to values fixed in the finite element model. These initial values can be assessed by several methods using ambient vibrations or natural/artificial generated low excitations on existing structures (e.g., MAVFRO techniques in Gaviria and Montejo (2016)). Table 1 outlined the initial values of matrices used in this research.

Table 1 Initial matrices of structural properties

Property	Mass × 103 [Kg]				Stiffness × 106 [N/m]				Damping × 106 [N s/m]			
DOF*	1	2	3	4	1	2	3	4	1	2	3	4
1	710				978	-495	106	-8	1.01	-0.31	0.01	-0.01
2		710				724	-444	86		0.78	-0.33	-0.01
3			710				641	-293			0.73	-0.30
4				710	SYM*			214	SYM*			0.39

*DOF: Degree of freedom; SYM: symmetric matrix

3. Numerical model

A state-of-the-art nonlinear numerical model of a four-story frame is considered for validation purposes of the proposed UKF scheme. The special moment frame has a typical story height of 3.96 m (156 in) and 4 spans of 9.14 m (360 in). Each column and beam has a section correspondingly of 0.864 × 0.965 m (34x38 in) and 0.864 × 1.070 m (34 × 30 in). Table 2 listed rebar distributions, geometric and nonlinear parameters of sections. The model is also loaded on each floor with a uniformly distributed dead-load of 42500 N/m (376 Kip/in).

In the Table 2, f'_c and f_{cu} denoted the maximum compression strength of concrete for unconfined and confined condition respectively; f_y and f_u are the characteristic stress of the steel (yielding and ultimate), the hinge length and equivalent inertia for the nonlinear finite elements analysis of concrete member is represented by L_p (Eq. (4)) and I_{eq}.

$$L_p = kL + 0.022 f_y d_{bl} \geq 2 * 0.0022 f_y d_{bl}, \qquad k = 0.2\left(\frac{f_u}{f_y} - 1\right) \leq 0.08 \tag{4}$$

where the diameter and length of longitudinal bars are d_{bl} and L correspondingly. The matlab script CUMBIA (Montejo and Kowalsky 2007) was used to perform the moment-curvature analysis of

Table 2 Reinforced concrete sections

Element	Geometric		Material properties				Reinforcement at the ends					Nonlinear parameters	
			Concrete		Steel		Longitudinal (number of bars #) bar size)			Transversal			
	Width [mm]	Height [mm]	f'_c [MPa]	f_{cu} [Mpa]	f_y [MPa]	f_u [MPa]	Top	Bot-tom	Intermediate	Bar size	As/S^* [mm^2/m]	L_p [mm]	I_{eq} [% of Ig]
Column	864	965	55.3	81.8	460	600	7#9	7#9	12#9	#4	7.24	580	35
Beam	864	762	41.5	48.0			8#10	8#9	6#4		1.84	653	41

*As: Area of transversal rebar; *S*: its separation

members and extract the values for I_{eq}.

OpenSees software was used as it allows to represent element sections by unidirectional fibers where each fiber can have a specific constitutive-material relationship. The material and element type used in the RC frame model are:

- *Concrete01* for concrete fiber (confined and unconfined) with the parameters defined by Mander *et al*. (1988).
  - *ReinforcingSteel* for longitudinal steel bars that take into account the degradation of stress during cyclic loads. The Coffin and Manson fatigue model (Mohle and Kunnath 2006) is integrated in this constitutive-material relationship and its defined by factors α, Cf, and Cd. These factors were taken as respectively 0.51, 0.15 and 0.45 and, were defined by Montejo (2008) from calibrated models of experimental tests of concrete columns with similar steel reinforcement distribution.
  - *Force-Based Beam-Column Element* is used to incorporate the strain softening of beam and column members. The Radau hinge integration method (Scott and Fenves 2006) is implemented in this type of element in order to force the occurrence of member plasticity within the assigned plastic hinge length.
  - *Elastic Beam-Column Element* is added to simulate strain penetration and the joint shear deformation (Priestley *et al*. 2007) on each node (or beam-column interface) because there is not joint shear failure in a RC frame designed according to modern seismic design codes (Haselton *et al*. 2008).

Also, P-Delta transformation and a 2% of proportional damping (tangent-stiffness) is considered in the model. Fig. 1 indicated the numeration of elements and the assigned type of element. The linear-elastic assembly of the model reported that the numerical model has periods of 1.19, 0.35, 0.17 and 0.11s for mode 1 to 4, correspondingly. And, condensed stiffness values of 406.30×10^3, 106.40×10^3, 55.10×10^3, and 35.70×10^3 kN/m associated with floor 1 to 4, respectively. The estimated response and properties of the model by the UKF scheme are normalized with the above values (Gaviria and Montejo 2019) as seen in section 2. Further detail

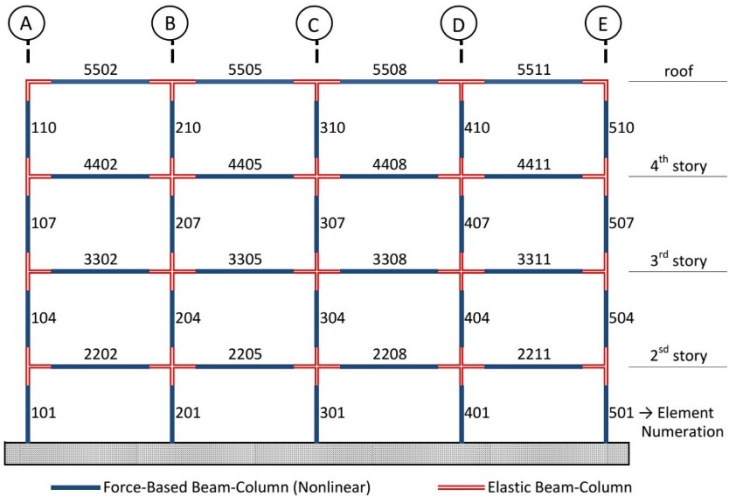

Fig. 1 Elevation view of the frame building and its type of finite element used

on the four-story structure can be found elsewhere (Haselton *et al*. 2011).

3.1 Earthquakes and seismic accelerations

An incremental dynamic analysis (IDA) is involved with a set of 3 seismic recorded accelerations to induce four different performance levels of the frame model. In order to represent from elastic performance to near collapse condition, the scale factors needed for each seismic record to reach story displacement-ductilities of 0.4, 2.0 and 4.0 as well as rupture of longitudinal reinforcement were determined (column 2 on Table 3). Fig. 2(a) shows that the highest structural ductility in the incremental dynamic analysis for the Gazli record is controlled by the first floor (continuous red line with circle markers). First floor inter-storey drifts from the IDA analysis for all records is presented in Fig. 2(b) and Table 3 presents the scaled factors and the physical and dynamic response parameters. From Fig. 2(b) is seen that the collapse condition (longitudinal rebar rupture) for the 1976 Gazli earthquake requires the largest ductility demand for all seismic records.

Table 3 shows that the natural frequencies exhibited by the structure after the earthquake do not tend to reflect a large increase in inelastic demand. The flat-file earthquake records used in this research can be accessed from the Next Generation Attenuation East (NGA-East, https://ngawest2.berkeley.edu/; last accessed October 2020)

Two different inter-story yield displacements (required to estimate the levels of inter-story ductility demand) were estimated, one for the first floor where the inelastic action is controlled by the hinges developed at the column base and one for all other floors where the hinges at beam ends control. The yield displacement for each story was estimated as the inter-store displacement required for the longitudinal reinforcement bars to reach the tensile strain required to fully develop the hinge. The required steel strain is estimated from an isolated moment-curvature analysis of the element in double bending, obtaining values of 0.0031 and 0.0035 for the bars in the columns and beams, respectively. The related inter-story yield displacement for the first and upper floors was 0.021 m (0.5 percent drift) and 0.036 m (0.9 percent drift), respectively. Using the concept of design displacement established by Priestley *et al*. (2007), the total structure ductility is determined as

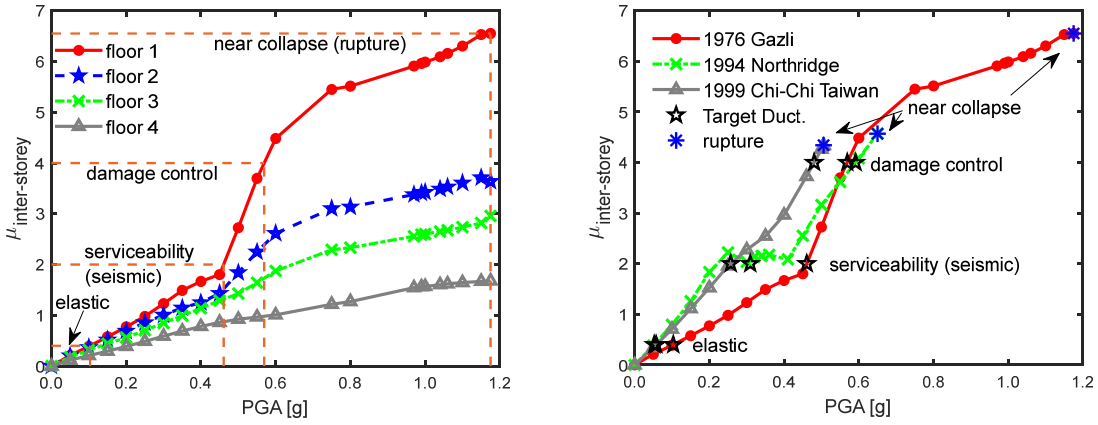

(a) 1976 Gazli record (b) All records (first storey only)

Fig. 2 Peak inter-story ductilities versus scaled factor (or PGA)

Table 3 Selected seismic recorded accelerations and key usefulness parameters

Ground motion name	Peak ground accel. (g)	Peak structural accel. (g)	Maximum inter-story μ	Maximum system μ	First frequency after EQ (Hz)	First period after EQ (s)*
1976 Gazli	0.10	0.18	0.42	0.35	0.82	1.22
Karakyir St. / 0°	0.46	0.69	2.36	1.61	0.74	1.35
	0.57	0.86	4.34	3.05	0.74	1.35
	1.18	1.55	8.74	6.02	0.74	1.36
1994 Northridge-1231	0.05	0.11	0.37	0.34	0.81	1.23
Lb-City Hall St./360°	0.31	0.45	2.25	1.71	0.76	1.32
	0.59	0.84	4.97	3.39	0.74	1.35
	0.65	0.93	5.76	3.94	0.74	1.35
1999 Chi-Chi Taiwan-03	0.06	0.15	0.39	0.35	0.84	1.20
TCU122 St/ East	0.26	0.44	2.49	1.78	0.75	1.33
	0.48	0.74	4.59	3.51	0.74	1.34
	0.51	0.77	5.57	4.00	0.74	1.35

*The fundamental period of undamaged structures is 1.19 s

$$\mu = \sum_{i=1}^{n} (m_i \mu_i{}^2) \Big/ \sum_{i=1}^{n} (m_i \mu_i) \tag{5}$$

In Eq. (5), m_i is the lumped mass and μ_i is the inter-story ductility at floor i. n is the number of stories. Inter-story and system ductility peak values are provided in Table 3. It is seen that the maximum inter-story ductility reached near to the collapse condition is between 5.57 and 8.74 are in agreement with the maximum value given by the direct design method for concrete structures (e.g., 7.00). Also, since the ground acceleration (column 2) is amplified by the structure (column 3) in all cases and the behaviour of IDA analysis for all records is different (Fig. 2(b)), the response of the four-story frame validates the selected earthquake records.

The resistivity to the noise is evaluated for typical low, intermediate and high noise levels (Turek and Ventura 2007) that correspond to 0.001 g, 0.005 g and 0.010 g root mean square (RMS) magnitudes. First, the noise time histories are generated and then, these signals are added to the output accelerations of the simulated responses previously to apply the UKF scheme.

4. Improved UKF-MDOF approach

The actual behavior of the structures may be mischaracterized by numerical models (Lund *et al.* 2020) and, this concern is especially important here because of the significance of the nonlinear dynamic behavior of the RC structures under severe damage induced by earthquake loads. If the initial matrices are not well approximated, KF performances end up in a suboptimal or even divergence way (Kuleli and Nagayama 2020). The expected extreme changes in the parameters and responses of the model are used to estimate the covariance of the noise process Q (Gaviria and

Montejo 2019). These variations may be computed using a diagonal Q matrix with small values of 10^{-25} through an initial UKF analysis of the undamaged SDOF system (Mariani and Ghisi 2007). However, due to the larger quantity of correlated variables on MDOF systems, an iterative scheme should be implemented to produce reliable results (Sen *et al*. 2018, Astroza *et al*. 2019). In this way, to determine the Q matrix to be used in the current UKF analysis, the recursive scheme used here takes the extreme response and parameters calculated in the previous iteration. The stop criterion is defined as a gap between the parameters calculated in the last 3 iterations of 5 percent or less. Also, a moving average is applied to estimated responses and parameters at each iteration prior to determining the maximum values in order to reduce spurious spikes in the retrieved responses. The smoothed applied has a duration (of moving average) of 90% of the first undamaged natural period of building that does not compromise the reliability of the results.

In addition, two criteria suggested in this paper ensure successful results of the provided UKF scheme:

- *Process covariance matrix* (*P*) *is penalized*: whereas the iterative scheme provided matrix Q that allows satisfactory range to capture the strong changes in modal and physical properties

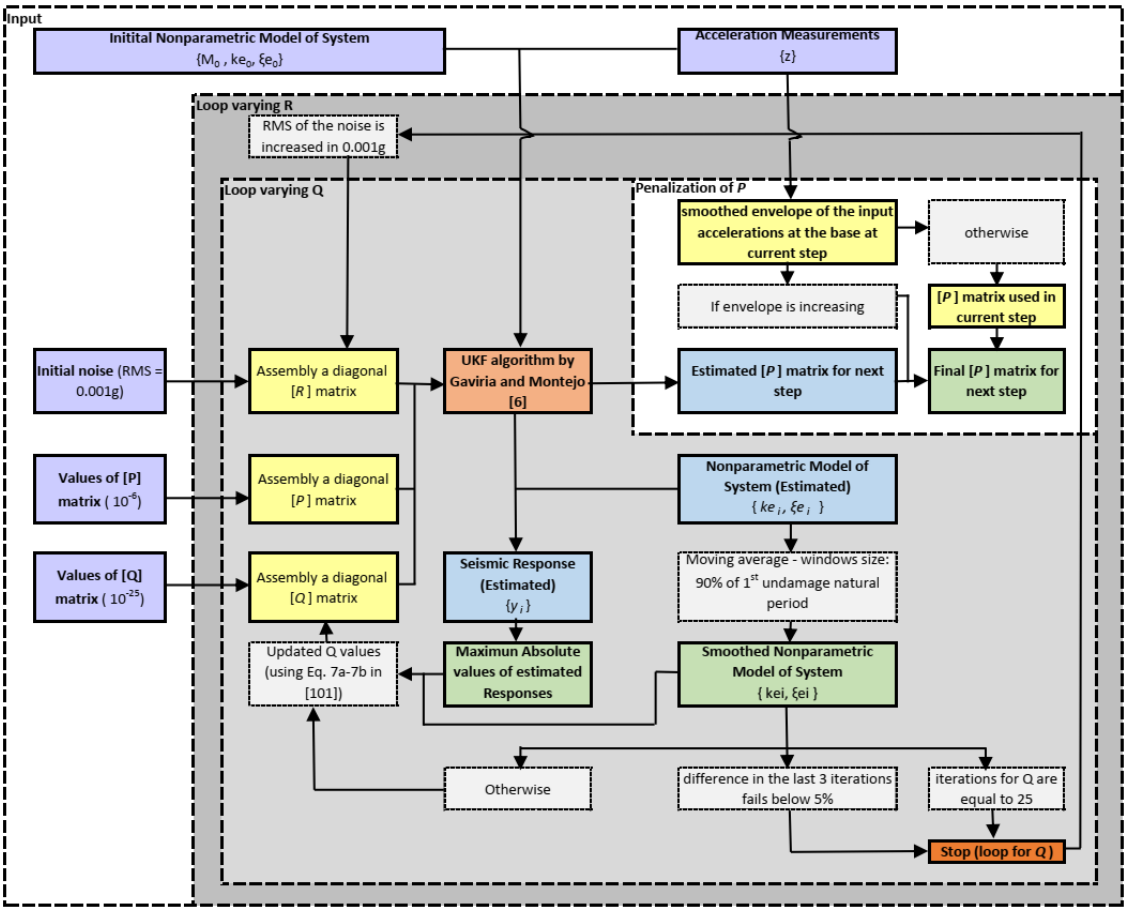

Fig. 3 Summary of the UKF-MDOF scheme

of structure, the effect of noise is critical when the system oscillates with a reduced amplitude compared to the maximum response achieved. A regulated evolution of P by the smoothed envelope of the input accelerations at the base is proposed to address this issue. Only if the input accelerations envelope increases, the values of matrix P would be allowed to increase.

- *The difference between the measurements and the estimated responses is augmented*: The accountable to allow an additional flexibility in UKF filters to consider the presence of noise is the measurement noise covariance matrix (R). An underestimated level of noise results in a low flexibility of the UKF to distinguish between a noise spurious peak response and a change in model parameters. To address this concern, an incremental iterative scheme is used as an outer loop of iterations for Q (as an inner loop) that start with a low level of noise of 0.001 g (RMS) as shown in Fig. 3. The stop criterion is defined as 25 iterations for Q where the difference between the parameters calculated in the last 3 iterations of greater than 5 percent. If this condition is satisfied, the RMS of the noise is increased in 0.001 g in the proposed iterative scheme for Q. Fig. 3 schematically illustrates the implementation of the improved UKF for MDOF systems. Readers are also referred to (Gaviria and Montejo 2019) for additional mathematical and implementation details.

The variation of responses and parameters using the RC frame response to the 1976 Gazli Earthquake scaled to 0.1 g (i.e., the structure achieves an inter-story ductility of 0.40) contaminated with noised (0.01 g of RMS) during the application of iterative UKF-MDOF framework is shown in Fig. 4. It is shown that after 12 (internal) iterations, the maximal values of responses (upper figures) and model parameters (bottom figures) converge (i.e., all curves reach a plateau at the 3 final steps). The final RMS used to calculate R was 0.005 g, i.e., it required 5 (outside) iterations. On all 48 analyses carried out (i.e., 3 ground motion to 4 scale factors and 4 noise levels), similar findings were obtained.

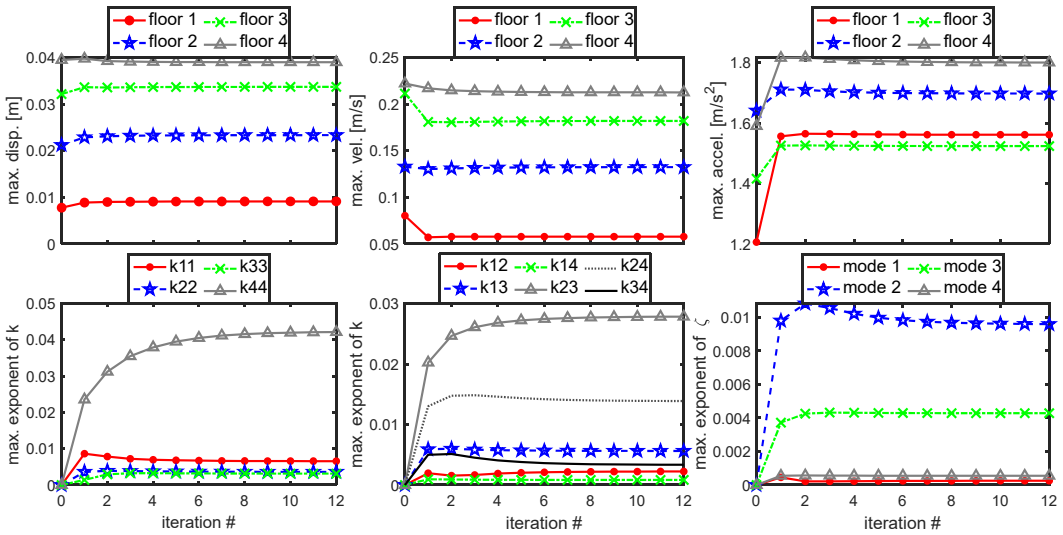

Fig. 4 Changes to the maximum values of responses and parameters of the structure the during the recursive UKF approach

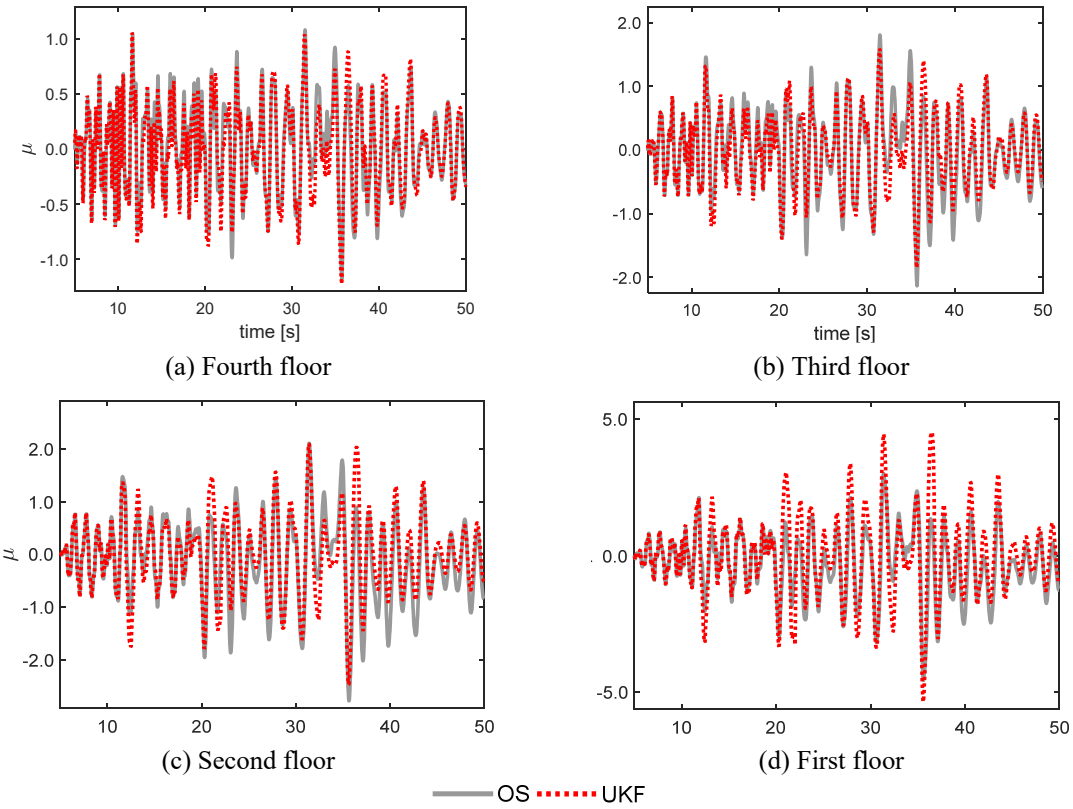

Fig. 5 Inter-story ductilities for story

5. Assessment of the UKF scheme proposed

The capacity of the aforementioned UKF methodology is tested on 48 scenarios. For the sake of brevity, this section explains the outcomes of the most difficult case that corresponds to 1994 Northridge ground motion with an amplitude of 0.65 g (PGA) and noise level of 0.01 g RMS where rebar fracturing takes place on the first level columns.

The displacements obtained by the proposed UKF expressed as inter-story ductility versus time are depicted in Fig. 5. It is shown seen that the displacements retrieved for the UKF scheme (dotted line) are in good agreement with the target response (i.e., the actual/simulated displacement identified as unbroken line and named OpenSees – OS) despite of high level of noise added to the simulated responses (0.01 g of RMS).

In order to compare the condensed stiffness matrix estimated by the UKF algorithm, one stiffness value kc_i per floor i is required (Cheng 2001) and it is being computed here. Thus, the full stiffness matrix assembly by nonlinear complex numerical model at each time step is reduced to four stiffness values (i.e., one per floor). The normalized results with the undamaged reduced stiffness of the RC frame are presented in Fig. 6. It is shown that the identified changes of the stiffness by floor follow the trend of the target values and the minimum values reached during the strong motion part of the earthquake are well captured, which are specifically important for the diagnosis of damage. Moreover, the long-term interval oscillation for values of condensed stiffness

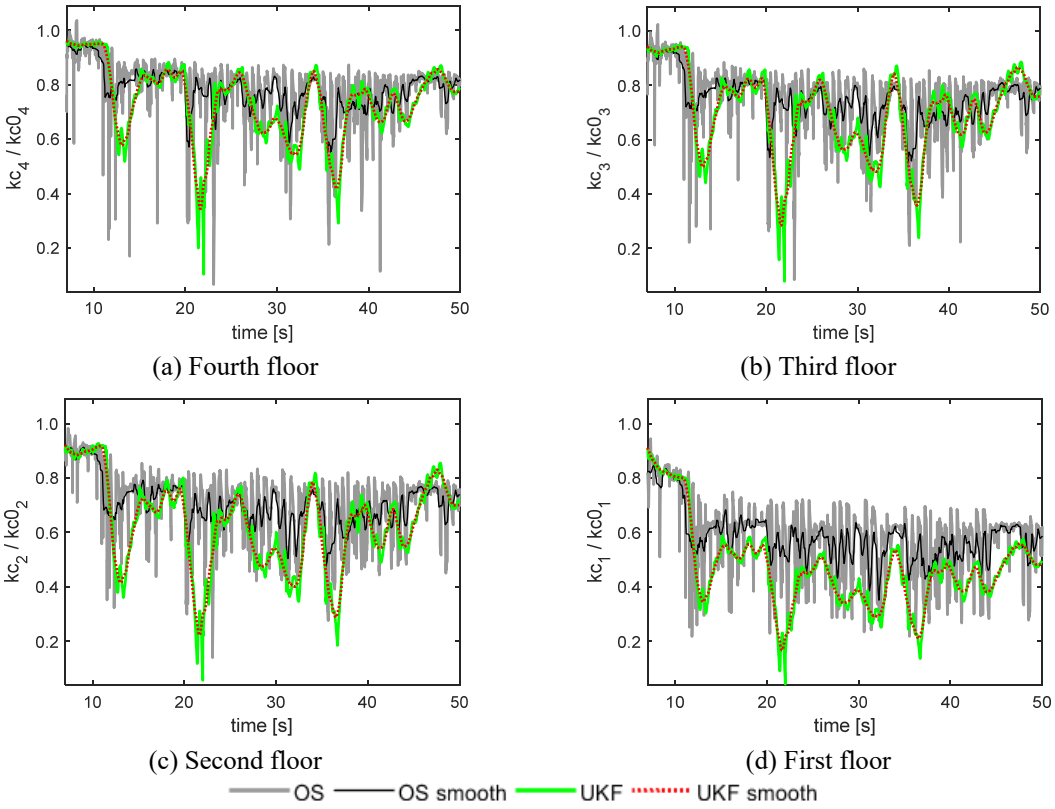

Fig. 6 Instantaneous normalized stiffness values per story

(i.e., when the vibration amplitude induced fade away) follow the shape of actual values. As is expected, major and permanent changes on condensed stiffness are observed at the first floor where the highest structural ductility takes place (see Fig. 2).

Four natural frequencies can be calculated in the proposed UKF-MDOF approach due to the fact that four DOF model (one per floor) is used to represent the RC frame. This is performed by computing the instantaneous eigenvalue values with the physical properties estimated at each time step. These values are compared with the actual/simulated first natural frequencies called OpenSees – OS in Fig. 7. It is shown that the UKF has superior tracking ability in the frequency of the first two modes that are more sensitive to the seismic load-induced damage. And, as we move to higher modes, the capability to identify instantaneous changes in frequencies is reduced. It is expected as well because the iterative UKF is updating the parameters of the system to match the modes that have higher contribution (fundamental modes) on the response. As for the stiffness estimation, the minimum and final values reached during the earthquake are close to the target for the first two modes. Moving on from the Fig. 6, it is seen that the minimum value of the stiffness (normalized with initial stiffness) reached during the seismic record is 18% compared to a minimum value of 50% of fundamental frequency achieved during the same scenario. These findings demonstrate that the variation of stiffness can depict small changes induced by damage or provide a better resolution of the magnitude of damage than the shifts in frequencies.

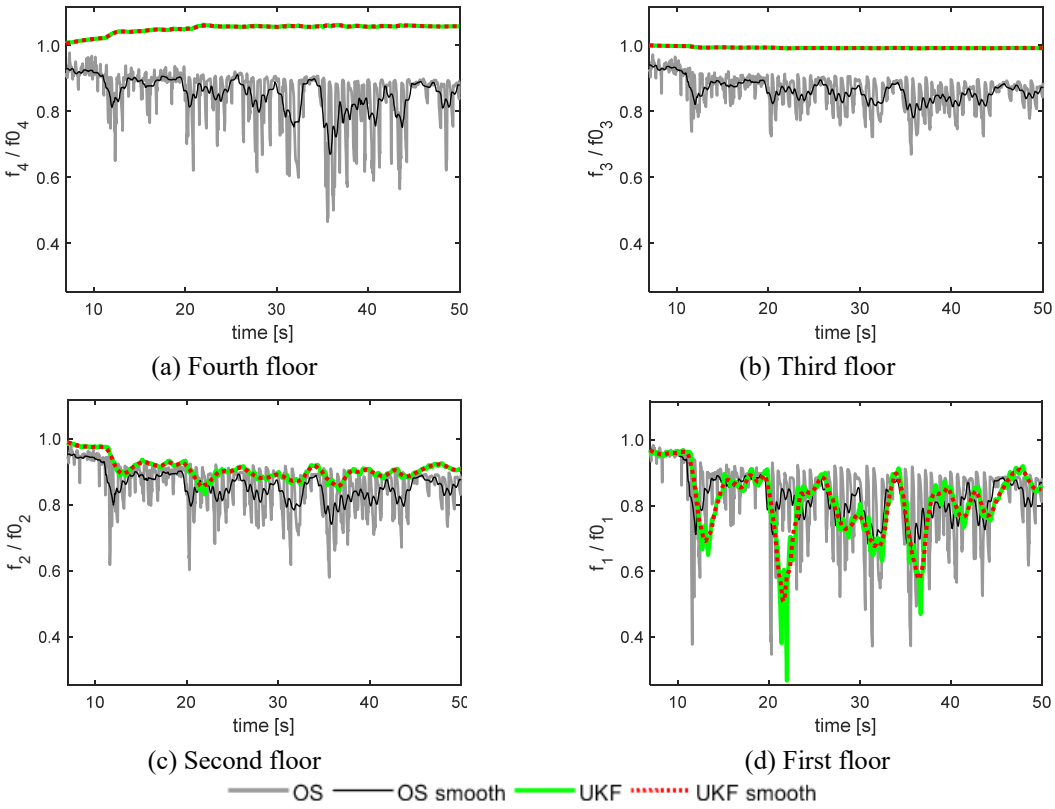

Fig. 7 Instantaneous normalized natural frequencies per mode

The structural model incorporated in the proposed UKF scheme calculates the instantaneous modal damping ratios as another advantage over a single initial or final value on vibration-based HSM (e.g., Gaviria and Montejo 2014, Ramírez and Montejo 2015). Thereby, the damping ratio of the whole system (ξ_{syst}) can be estimated as a pondered combination of n modal damping ratios (ξ_i) using the modal participation factors (Γ_i) of each i^{th} mode

$$\xi_{syst} = \sum_{i=1}^{n} \Gamma_i \xi_i \tag{6}$$

Eq. (6) was implemented within the UKF scheme to provide the instantaneous value of the damping ratio of the system. For comparison purposes, an expression of the analogous viscous damping applied to RC frame structures suggested by Grant *et al*. (2005) can be invoked

$$\xi_{eq} = \mu^{\lambda} \xi_{el} + a\left(1 - \frac{1}{{\mu_{max}}^{b}}\right) \tag{7}$$

This equation combines the elastic damping ratio (ξ_{el}), the peak system ductility (μ) corrected by the factor λ (equal to *-0.313*) and the Takeda-Fat" hysteretic model (with a = *0.305* and b= *0.492*). This is the equivalent viscous damping of an analogous SDOF model of a MDOF structure

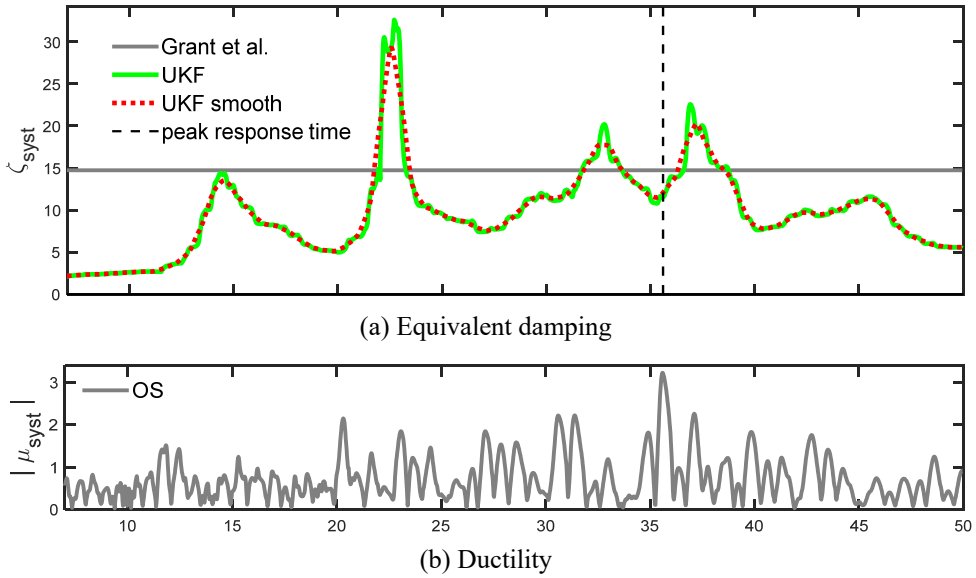

(a) Equivalent damping

(b) Ductility

Fig. 8 Variations in the estimated parameters of the whole system

that is defined on direct-displacement design of RC structures where the primary response is determined by the fundamental inelastic mode (Priestley *et al*. 2007). Fig. 8(a) shows the variation of the estimated damping ratio of the system. The instantaneous damping ratio of the whole system is fluctuating around the equivalent viscous damping ratio (for the peak system ductility condition). The damping remains below 10% with an average value of 3% before the first inelastic episode (at 12 s), as expected for low amplitudes where ductility remain close to 1.0 (Fig. 8(b)). This value increases due to the hysteretic damping contributions after large levels of displacement demand. Moreover, peak damping values of 30%, 18% and 20% are observed at 22, 33 and 37s that are consistent with spikes reported on stiffness and frequency results (Figs. 6-7). During these times, the RC frame is subjected nonlinear excursions which are recognized by the proposed UKF-MDOF approach by coping the reduction in the post-peak amplitude of the vibrations with additional damping. These peaks can be useful to identify the time location of damage episodes.

6. Damage analysis

Previous section argued the results of proposed iterative UKF-MDOF approach for identification of instantaneous physical and modal properties of the RC frame structure. The capacity of these results as damage measurements for all seismic scenarios with a medium noise level (i.e., 0.005 g of RMS) is explored in this section.

The minimum values of condensed stiffness per floor and the stiffness at the end of earthquake normalized with its undamaged initial values are depicted in Fig. 9. Based on Figs. 9(a) and (b), a good correlation between the reached maximum displacement and both types of stiffness indicators at the first floor is observed. Nevertheless, the change in stiffness exhibited by the structure after the earthquake to saturate once the structure reaches ductility one. Comparison of the results show that the constant exponent terms of the fitting exponential curves have the largest values when the minimum values of the stiffness are used (i.e., negative constant values between

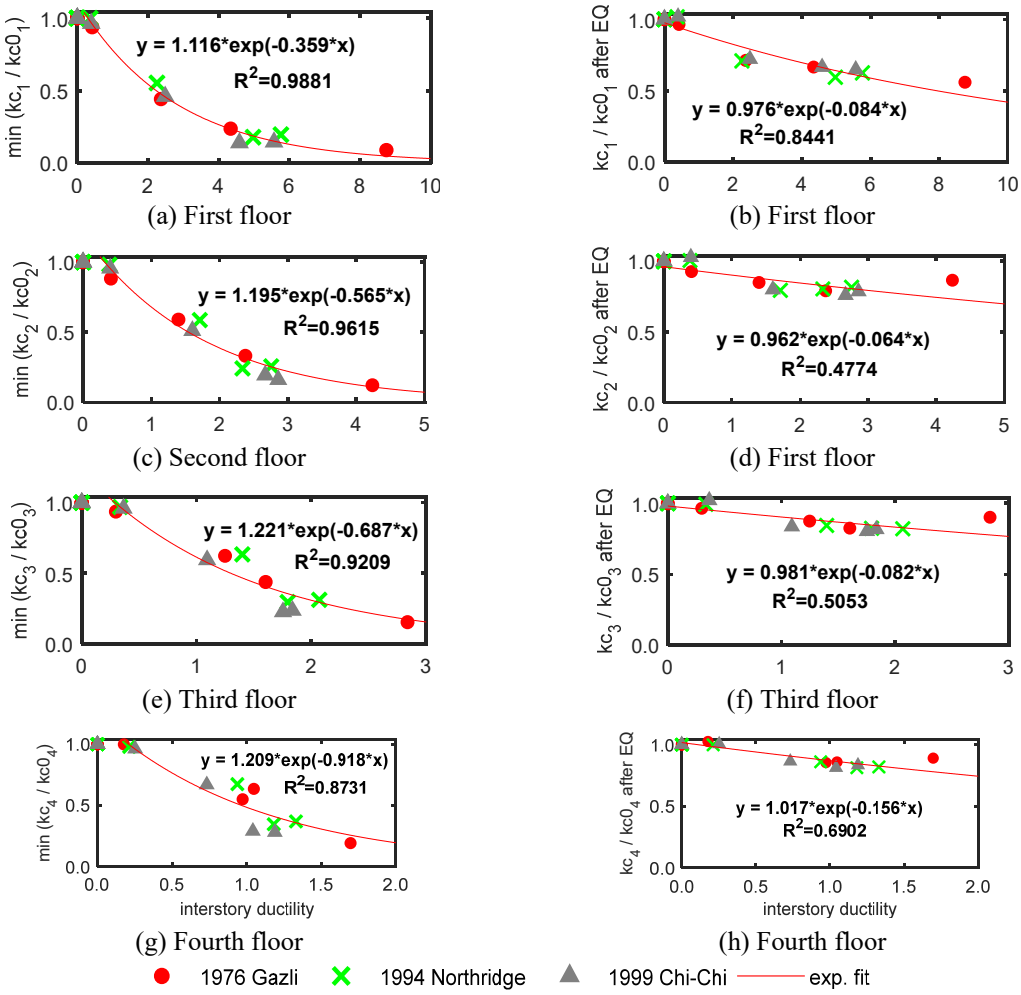

Fig. 9 Comparative of minimum stiffness reached during the ground motion (left) and the post-earthquake stiffness (right) with the ductility demand

0.359 and 0.918). As is expected the absolute value of exponential constant part in the equation increases as we move up on the floors, which is consistent with the reduction on ductility demand reached by its corresponding level (see Figs. 9(a), (c), (e) and (g)). Also, the minimum value of stiffness results by floor exhibit the largest values of R^2.

Fig. 10 shows the minimum first natural frequency reached by the structure during each earthquake excitation and the frequency exhibited by the structure after the earthquake as function of the maximum ductility reached by the structure during the excitation. It is seen that the changes of minimum value of natural frequency correlated well with both the level of inelastic demand and have the largest values of R^2 (values higher than 0.90, see Figs. 10(a) and (b)). Moreover, the same pattern observed for the condensed stiffness values is appreciated: minimum frequency values show to be more sensitive than post-earthquake frequency values. The largest constant exponent term of the fitting exponential curves is reported for the system ductility (absolute value of 0.204). Comparison of the constant exponent terms with the stiffness results in Fig. 9 show that the

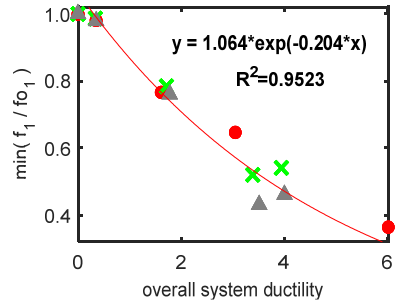

(a) Minimum natural frequency vs the system ductility

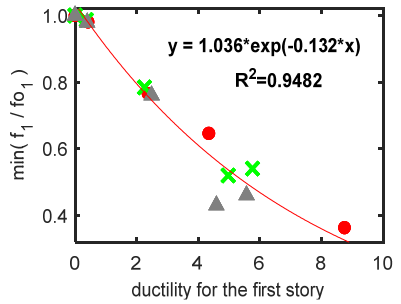

(b) Minimum natural frequency vs the ductility of the first floor

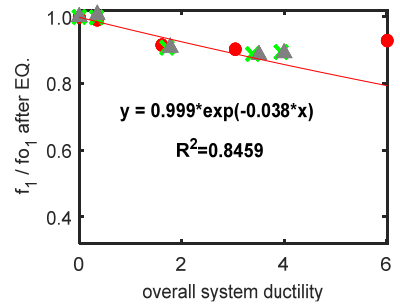

(c) Post-earthquake natural frequency vs system ductility

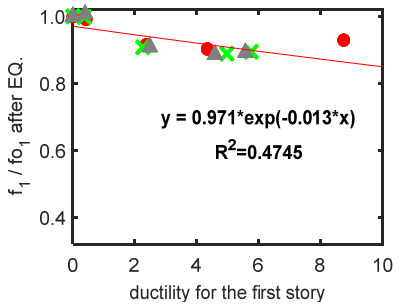

(d) Post-earthquake natural frequency vs the ductility of the first floor

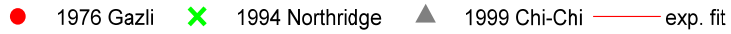

Fig. 10 Comparative of minimum natural frequency reached during the ground motion (top) and the post-earthquake natural frequency (bottom) with both types of ductility demands

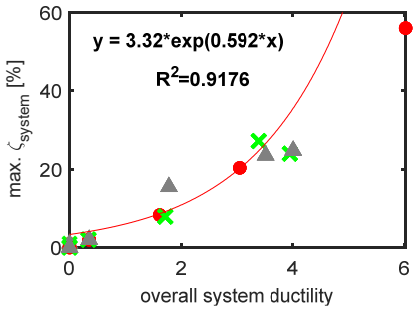

(a) Maximum-equivalent damping vs the system ductility

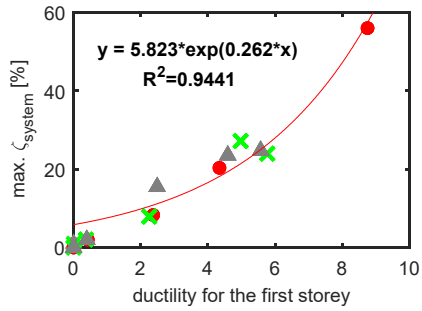

(b) Maximum-equivalent damping vs the ductility of the first floor

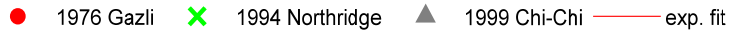

Fig. 11 Comparative of total damping (maximum-equivalent) with both types of ductility demands

minimum stiffness is more sensitive to changes of the maximum displacement values reached by the structure (absolute values higher than 0.359). In the case of post-earthquake frequency (Figs. 10(c, d)), the fitting of exponential curves are not correlated appropriately with the actual value for

the largest value of ductility demand.

Finally, the peak values of damping ratio of the overall system estimated by the UKF approach during each earthquake scenario is presented in Fig. 11. It is shown that the peak damping values are in agreement with the ductility demand of the system and the principal local ductility (i.e., ductility of the first floor). The damping ratio is correlated more appropriately with the ductility of the first story (see Fig. 11(b)) and has a larger value of R^2 than that of the system ductility that is associated with the concentration of energy dissipation at the first floor of the structure. In the case of system ductility (Fig. 11(a)), the exponential regression is distant for the highest value of ductility reported. Also, the correlation between minimum values of stiffness and the normalized first natural frequency with interstory ductility initiated from a value of 1.0 and, the correlation between the maximum equivalent damping ratios and the ductility for the first floor initiated from a value of 5.8 that is the minimum total damping of the studied RC frame.

7. Conclusions

This study presents an extended UKF scheme (Gaviria and Montejo 2019) for the identification of the structural properties of RC structures under different levels of inelastic demand levels by seismic loads. The approach is evaluated using numerical responses from a state of the art fiber-based nonlinear model of a 4-story 4-bays RC frame. The responses used range from elastic to near to collapse condition providing rebar fracture episodes. The noise resistance is considered by adding different levels of noise in order to reproduce raw data on field conditions.

- The estimated parameters and responses obtained by the UKF scheme are determined by its statistical parameters that need to adjust the UKF to the ductility demand induced by a particular seismic load (Gaviria and Montejo 2019, Kuleli and Nagayama 2020). Thus, the Q and R matrixes are computed through a new approach that adapts the statistical parameters. Results are shown that the assessed physical/modal properties are consistent with current values from numerical simulated behavior.
- The modal response reconstructed by the proposed UKF scheme were shown to be guide by the first dominant modes and a limited capacity for tracking the frequency of upper modes. This result is anticipated because the participation of higher modes on structure response is disappear faster and have less amplitude than lower modes (e.g., Gaviria and Montejo 2019, Montejo and Vidot-Vega 2012). In spite of this, the instantaneous deformation shape of the structure is well retrieved, ensuring an adequate story drift-based damage identification.
- The estimated response and parameters at each time step by the presented method provides a broad range options of damage indicators (global and local) on RC structures under high nonlinear behavior induced by earthquakes. The instantaneous floor displacements are a direct measure of damage episodes and, their locations and magnitude per story. The stiffness and frequency after each earthquake revealed a restricted capacity to pursue the ductility achieved by the structure. However, the minimum values of these properties during the seismic movement were shown to be proportional to the induced ductility demand which results in more appropriate damage measurements.
- Finally, the time variation of equivalent damping ratio identified by the unscented Kalman filter followed the pattern of overall and first floor inelastic ductility demand in the

structure and, it will be an indicator really worth of future research. As these identification algorithms progress beyond state-of-the-art simulation results to implementations, additional research is needed to validate the proposed HSM scheme when using data recorded from actual structures.

Acknowledgments

This research is supported by the National Science Foundation Grant No. CMMI-1121146. Any opinions, findings and conclusions or recommendations expressed in this study are those of the writers and do not necessarily reflect the views of the National Science Foundation. The authors also acknowledge to the University of Puerto Rico at Mayaguez and Universidad Militar Nueva Granada.

References

Aguirre, D.A., Gaviria, C.A. and Montejo, L.A. (2013), "Wavelet-based damage detection in reinforced concrete structures subjected to seismic excitations", *J. Earthq. Eng.*, **17**(8), 1103-1125. https://doi.org/10.1080/13632469.2013.804467

Astroza, R. and Alessandri, A. (2019), "Effects of model uncertainty in nonlinear structural finite element model updating by numerical simulation of building structures", *Struct. Control Health Monitor.*, **26**(3), e2297. https://doi.org/10.1002/stc.2297

Astroza, R., Ebrahimian, H. and Conte, J.P. (2017), "Batch and recursive Bayesian estimation methods for nonlinear structural system identification", In: *Risk and Reliability Analysis*: *Theory and Applications*, Springer, Cham, Switzerland.

Astroza, R., Barrientos, N., Li, Y., Flores, E.I. and Liu, Z. (2019), "Bayesian updating of complex nonlinear FE models with high-dimensional parameter space using heterogeneous measurements and a batch-recursive approach", *Eng. Struct.*, **201**, e109724. https://doi.org/10.1016/j.engstruct.2019.109724

Astroza, R., Barrientos, N., Li, Y. and Flores, E.S. (2020), "Calibration of a large nonlinear finite element model of a highway bridge with many uncertain parameters", In: *Validation and Uncertainty Quantification*, 3rd ed., Springer, Cham, Switzerland.

Azam, S.E. and Mariani, S. (2018), "Online damage detection in structural systems via dynamic inverse analysis: A recursive Bayesian approach", *Eng. Struct.*, **159**, 28-45. https://doi.org/10.1016/j.engstruct.2017.12.031

Azam, S.E., Mariani, S. and Attari, N.K. (2017), "Online damage detection via a synergy of proper orthogonal decomposition and recursive Bayesian filters", *Nonlinear Dyn.*, **89**(2), 1489-1511. https://doi.org/10.1007/s11071-017-3530-1

Bocciarelli, M. and Ranzi, G (2020), "Stochastic and recursive estimation of the hygro-thermo-chemical-mechanical parameters of concrete through Monte Carlo analysis and extended Kalman filter", *Struct. Multidisc. Optim.*, **61**, 91-110. https://doi.org/10.1007/s00158-019-02347-y

Consuegra, F. and Irfanoglu, A. (2008), "Variation of dynamic properties with displacement in a 3-story reinforced concrete flat plate structure", *Proceedings of the 14th World Conference on Earthquake Engineering*, Beijing, China, October.

Cheng, F.Y. (2001), *Matrix Analysis of Structural Dynamics*: *Applications and Earthquake Engineering*, Marcel Dekker Inc., New York, NY, USA.

De Roeck, G. (2019), "Model–based methods of damage identification of structures under seismic excitation", In: *Seismic Structural Health Monitoring*, Springer, Cham, Switzerland.

Gaviria, C.A. (2015), "A computational framework for structural health monitoring of reinforced concrete structures", Ph.D. Dissertation; University of Puerto Rico, Mayaguez.

Gaviria, C.A. and Montejo, L.A. (2014), "Wavelet based damping identification from noise contaminated signals", *Proceedings of the 10th National Conference in Earthquake Engineering*, Anchorage, AL, USA, July. https://doi.org/10.4231/D3S17ST11

Gaviria, C.A. and Montejo, L.A. (2016), "Output-only identification of the modal and physical properties of structures using free vibration response", *Earthq. Eng. Eng. Vib.*, **15**(3), 575-589. https://doi.org/10.1007/s11803-016-0345-x

Gaviria, C.A. and Montejo, L.A. (2018), "Optimal wavelet parameters for system identification of civil engineering structures", *Earthq. Spectra*, **34**(1), 197-216. https://doi.org/10.1193/092016EQS154M

Gaviria, C.A. and Montejo, L.A. (2019), "Monitoring physical and dynamic properties of reinforced concrete structures during seismic excitations", *Constr. Build. Mater.*, **196**, 43-53. https://doi.org/10.1016/j.conbuildmat.2018.11.106

Ghanem, R. and Ferro, G. (2006), "Health monitoring for strongly non-linear systems using the Ensemble Kalman filter", *Struct. Control. Health Monitor.*, **13**, 245-259. https://doi.org/10.1002/stc.139

Grant, D.N., Blandon, C.A. and Priestley, M.J.N. (2005), *Modeling Inelastic Response in Direct Displacement-Based Design*, IUSS Press, Pavia, Italy.

Haselton, C.B., Goulet, C.A., Mitrani-Reiser, J., Beck, J.L., Deierlein, G.G., Porter, K.A., Stewart, J.P. and Taciroglu, E. (2008), "An Assessment to Benchmark the Seismic Performance of a Code-Conforming Reinforced-Concrete Moment-Frame Building", Pacific Earthquake Engineering Research Center, August.

Haselton, C.B., Liel, A.B., Deierlein, G.G., Dean, B.S. and Chou, J.H. (2011), "Seismic collapse safety of reinforced concrete buildings. I: Assessment of ductile moment frames", *J. Struct. Eng.*, **137**(4), 481-491. https://doi.org/10.1061/(ASCE)ST.1943-541X.0000318

He, H., Lv, Y. and Han, E. (2014), "Damage detection for continuous bridge based on static-dynamic condensation and extended Kalman filtering", *Math. Probl. Eng.*, **7**, 1-14. https://doi.org/10.1155/2014/707969

He, L.X., Wu, C. and Li, J. (2019), "Post-earthquake evaluation of damage and residual performance of UHPSFRC piers based on nonlinear model updating", *J. Sound Vib.*, **448**, 53-72. https://doi.org/10.1016/j.jsv.2019.02.011

Humar, J. (2012), *Dynamics of Structures*, 3rd ed., CRC press, Taylor & Francis Group, London, England.

Julier, S.J. and Uhlmann, J.K. (1997), "A new extension of the Kalman filter to nonlinear systems", *Proceedings of AeroSense 97 Conference on Photonic Quantum Computing*, Orlando, FL, USA, April. https://doi.org/10.1117/12.280797

Katkhuda, H., Shatarat, N. and Hyari, K. (2017), "Two-stage system identification approach for three-dimensional structural systems", *Int. J. Struct. Eng.*, **8**(2), 93-110. https://doi.org/10.1504/IJSTRUCTE.2017.084628

Kuleli, M. and Nagayama, T. (2020), "A robust structural parameter estimation method using seismic response measurements", *Struct. Control Health Monitor.*, **27**(3), e2475. https://doi.org/10.1002/stc.2475

Li, Y., Astroza, R., Conte, J.P. and Soto, P. (2017), "Nonlinear FE model updating and reconstruction of the response of an instrumented seismic isolated bridge to the 2010 Maule Chile earthquake", *Earthq. Eng. Struct. Dyn.*, **46**(15), 2699-2716. https://doi.org/10.1002/eqe.2925

Lund, A., Dyke, S.J., Song, W. and Bilionis, I. (2019), "Global sensitivity analysis for the design of nonlinear identification experiments", *Nonlinear Dyn.*, **98**(1), 375-394. https://doi.org/10.1007/s11071-019-05199-9

Lund, A., Dyke, S.J., Song, W. and Bilionis, I. (2020), "Identification of an experimental nonlinear energy sink device using the unscented Kalman filter", *Mech. Syst. Sig. Process.*, **136**, 106512. https://doi.org/10.1016/j.ymssp.2019.106512

Mander, J., Priestley, M. and Park, R. (1988), "Theoretical Stress-Strain Model for Confined Concrete", *J. Struct. Eng.*, **114**(8), 1804-1826. https://doi.org/10.1061/(ASCE)0733-9445(1988)114:8(1804)

Mariani, S. and Ghisi, A. (2007), "Unscented Kalman filtering for nonlinear structural dynamics", *Nonlinear Dyn.*, **49**, 131-150. https://doi.org/10.1007/s11071-006-9118-9

Masri, S.F., Caffrey, J.P., Caughey, T.K., Smyth, A.W. and Chassiakos, A.G. (2004), "Identification of the state equation in complex non-linear systems", *Int. J. Non-Linear Mech.*, **39**(7), 1111-1127.

https://doi.org/10.1016/S0020-7462(03)00109-4
Mohle, J. and Kunnath, S. (2006), Reinforcing Steel Material. OpenSees user's manual, July.
Montejo, L.A. (2008), "Seismic behavior of reinforced concrete bridge columns at sub-freezing temperatures", Ph.D. Dissertation; North Carolina State University, Raleigh, USA.
Montejo, L.A. and Kowalsky, M.J. (2007), "CUMBIA—Set of Codes for the Analysis of Reinforced Concrete Members", CFL Technical Report No. IS-07; North Carolina State University, Raleigh, USA.
Montejo, L.A. and Kowalsky, M.J. (2008), "Estimation of frequency-dependent strong motion duration via wavelets and its influence on nonlinear seismic response", *Comput.-Aided Civil Infrastruct. Eng.*, **23**(4), 253-264. https://doi.org/10.1111/j.1467-8667.2007.00534.x
Montejo, L.A. and Vidot-Vega, A.L. (2012), "Synchrosqueezed wavelet transform for frequency and damping identification from noisy signals", *Smart Struct. Syst., Int. J.*, **9**(5), 441-459. https://doi.org/10.12989/sss.2012.9.5.441
Montejo, L.A., Gaviria, C.A. and Aguirre, D.A. (2015), "Tracking dynamic properties of civil structures while subjected to seismic excitations", *Proceedings of the 11th Canadian Conference on Earthquake Engineering*, Victoria, Canada, July.
Murillo, M.J., Gaviria, C.A., Cantillo, Y.A. and Acosta, C.A. (2019), "A low-cost approach to monitoring the structural health of pedestrian bridges", *Revista Espacios*, **40**(27), 14-23.
Priestley, M., Calvi, G. and Kowalsky, M. (2007), *Direct Displacement-Based Seismic Design of Structures*, IUSS Press, Pavia, Italy.
Qiu, Q. and Lau, D. (2021), "Defect detection of FRP-bonded civil structures under vehicle-induced airborne noise", *Mech. Syst. Sig. Process.*, **146**, 1069. https://doi.org/10.1016/j.ymssp.2020.106992
Quiñones, M.M., Montejo, L.A. and Jang, S. (2015), "Experimental and numerical evaluation of wavelet based damage detection methodologies", *Int. J. Adv. Struct. Eng.*, **7(**1), 69-80. https://doi.org/10.1007/s40091-015-0084-7
Ramírez, R.I. and Montejo, L.A. (2015), "On the identification of damping from non-stationary free decay signals using modern signal processing technique", *Int. J. Adv. Struct. Eng.*, **7**(3), 321-328. https://doi.org/10.1007/s40091-015-0096-3
Roohi, M., Hernandez, E.M. and Rosowsky, D. (2021), "Reconstructing Element-by-Element Dissipated Hysteretic Energy in Instrumented Buildings: Application to the Van Nuys Hotel Testbed", *J. Eng. Mech.*, **147**(1), 04020141. https://doi.org/10.1061/(ASCE)EM.1943-7889.0001864
Scott, M. and Fenves, G. (2006), "Plastic Hinge Integration Methods for Force-Based Beam–Column Elements", *J. Struct. Eng.*, **132**(2), 244-252. https://doi.org/10.1061/(ASCE)0733-9445(2006)132:2(244)
Sen, S., Crinière, A., Mevel, L., Cérou, F. and Dumoulin, J. (2018), "Seismic-induced damage detection through parallel force and parameter estimation using an improved interacting Particle-Kalman filter", *Mech. Syst. Sig. Process.*, **110**, 231-247. https://doi.org/10.1016/j.ymssp.2018.03.016
Song, W. and Dyke, S. (2014), "Real-time dynamic model updating of a hysteretic structural system", *J. Struct. Eng.*, **140**(3), 201-214. https://doi.org/10.1061/(ASCE)ST.1943-541X.0000857
Turek, M. and Ventura, C.E. (2007), "Calibrated vibration simulations for design of SHM systems", In: *IMAC XXV*: *Conference & Exposition on Structural Dynamics*, Orlando, FL, USA, February.
Wan, Z., Wang, T., Li, S. and Zhang, Z. (2018), "A modified particle filter for parameter identification with unknown inputs", *Struct. Control Health Monitor.*, **25**(12), e2268. https://doi.org/10.1002/stc.2268
Wu, B. and Wang, T. (2014), "Model updating with constrained unscented Kalman filter for hybrid testing", *Smart Struct. Syst., Int. J.*, **14**(6), 1105-1129. https://doi.org/10.12989/sss.2014.14.6.1105
Yazdanpanah, O., Mohebi, B. and Yakhchalian, M. (2020), "Selection of optimal wavelet-based damage-sensitive feature for seismic damage diagnosis", *Measurement*, **154**, 107447. https://doi.org/10.1016/j.measurement.2019.107447